rates ranging from 16 ft/day down to 0.16 ft/day. It should be pointed out that there is no unanimous agreement on the lower limit of flow where diffusion may be neglected. For example, in the range between 0.1 to 0.5 ft/day, the diametrically opposed conclusion, namely, that molecular diffusion is the dominant factor, has also been reached.[18] Experimental investigations in this area continue to be made.

Where molecular diffusion is negligible the present theory predicts, as may be seen by comparing Eqs. (6.8) and (6.9), that the "effective diffusion constant" $\mathfrak{D}$ is approximately proportional to the rate of flow. Experimental evidence confirms this rather well.[18,20] In the extreme case of no macroscopic flow, our equations break down. However, even at the very small flow rates where molecular diffusion is predominant, they still may be used to describe the observed effects if a proper value of D is selected, so as to make Eqs. (6.8) and (6.9) identical. From the phenomenological point of view, the general equation [Eq. (3.2)] offers greater flexibility than the conventional diffusion equation, through the choice of two adjustable parameters.

d. A similar theory also may be applied to other displacement processes such as the replacing of one kind of ion by another in ion-exchange columns. This was done by Thomas,[19] in dealing with the kinetics of ion exchange and chromatography, and by Polya[20] to treat the analogous problem of gravel transport by rivers.

ACKNOWLEDGMENT

I wish to thank Dr. G. H. F. Gardner for his comments which formed the basis of the discussion in Sec. 6.

[18] R. J. Blackwell, J. R. Rayne, and W. M. Terry, J. Petrol. Technol., XI, 1 (January, 1959).
[19] H. C. Thomas, J. Am. Chem. Soc. 66, 1664 (1944), and Ann. N. Y. Acad. Sci. 49, 161 (1948).
[20] G. Polya, *Zur Kinematik der Geschiebebewegung* (Mitteilung der Versuchsanstalt für Wasserbau an der Eidg. Techn. Hochschule, Zürich, Switzerland, 1937).

THE PHYSICS OF FLUIDS VOLUME 3, NUMBER 2 MARCH-APRIL, 1960

Shock Hugoniots for Liquid Argon

W. FICKETT AND W. W. WOOD
Los Alamos Scientific Laboratory, University of California, Los Alamos, New Mexico
(Revised September 28, 1959)

Shock Hugoniots for liquid argon are calculated using equations-of-state obtained from the Monte Carlo method and the Lennard-Jones-Devonshire cell theory, using an experimentally determined pair potential. Agreement with presently available experimental data is poor.

1. INTRODUCTION

MANY statistical mechanical theories of the equation of state of dense molecular systems make use of the assumption of additivity of intermolecular forces, which states that the total interaction energy can be expressed as a sum of terms referring to the interactions of isolated pairs of molecules. It is known that this assumption is not exactly correct, and the degree of its validity has been the subject of considerable investigation.[1] However, there is very little, if any, experimental information pertaining to the repulsive region of the pair potential of intermolecular force.

The additivity assumption can of course be tested by comparing with experiment the results of statistical calculations based on experimentally determined pair potentials. From the theoretical standpoint, this approach has been hindered by the lack of accurate data on the repulsive portion of the pair potential, and of an accurate and tractable statistical theory. These difficulties have been partly overcome in recent years. The molecular scattering method for the determination of pair potentials has been extended out to distances near the crossover,[2] and the Monte Carlo method of calculation[3] is free of the major uncertainties in

[1] L. Jansen, *Some Aspects of Molecular Interactions in Dense Media* (Martinus Nijhoff, The Hague, Netherlands, 1955).
[2] I. Amdur and E. A. Mason, J. Chem. Phys. 22, 670 (1954); Phys. Fluids 1, 370 (1958).
[3] W. W. Wood and F. R. Parker, J. Chem. Phys. 27, 720 (1957) (further results are to be published).

the usual statistical theories of the equation of state. On the experimental side, the high compressions required can be reached by means of shock waves generated by condensed explosives. Pressure and volume can be obtained from measurements of shock and particle velocity,[4] or by x-ray densitometry.[5] Since the compression takes place along a Hugoniot curve, however, a considerable rise in temperature is unavoidable.

Liquid argon would appear to be the material of choice. The pair potential is spherically symmetric, and its repulsive portion has been experimentally determined in the appopriate range of distances.[2] Monte Carlo equation-of-state calculations[3] have been done for a form of the pair potential and a range of reduced temperatures and volumes which are appropriate, and some points on the shock Hugoniot have been measured.[5]

Accordingly, the calculations presented here are for the shock Hugoniot of liquid argon. They are based on the experimentally determined repulsive portion of the pair potential and the Monte Carlo calculation of the equation of state. Since the Monte Carlo calculations are expensive in computer time, and were done with a somewhat different pair potential, the Lennard-Jones-Devonshire (LJD) cell model equation-of-state[6] is used as a substitute for the Monte Carlo method in order to calculate the Hugoniot with the experimental pair potential. The Hugoniots calculated from the LJD and Monte Carlo equations of state with the same pair potential agree surprisingly well, and thus afford some confidence in this procedure.

2. COMPARISON OF MONTE CARLO AND LENNARD-JONES-DEVONSHIRE EQUATIONS OF STATE

The model used is a system of argon atoms in the ground state. As discussed above, the additivity of pair forces is assumed throughout.

The shock Hugoniot curve is the solution of the equation[7]

$$E - E_0 - \tfrac{1}{2}P(V_0 - V) = 0 \qquad (2.1a)$$

$$E = \tfrac{3}{2}R(T - T_0) + E', \qquad (2.1b)$$

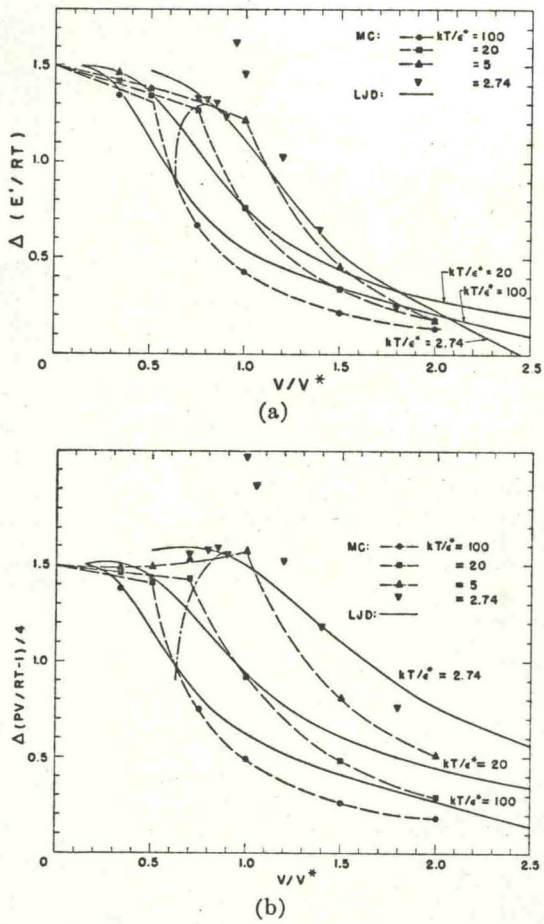

FIG. 1. Isotherms for the Monte Carlo (points and dashed curves) and LJD (solid curves) equations of state. Excess quantities over those for the regular (face-centered cubic) lattice configuration are shown (see text). The chain curves show the approximate position of the shock Hugoniot.

where P, V, and E are the pressure, molar volume, and molar internal energy, respectively, and the subscript $_0$ denotes the initial state, which is taken to be liquid argon at its boiling point:[8] $P_0 = 1$ atm; $V_0 = 28.7$ cm^3/mole; $T_0 = 87.29$ °K; and $E_0/RT_0 = -7.982$, where the reference state for the energy is gaseous argon in the ideal gas state at T_0. (We have taken $E_0/RT_0 = \Delta H_v/RT_0 - 1$, with ΔH_v the experimental enthalpy of vaporization at T_0.) The imperfection energy E' is calculated from the LJD cell theory or the Monte Carlo method.

The Monte Carlo technique has been used to generate points on four isotherms,[3] using the Lennard-Jones 6–12 form for the pair potential;

$$u(r) = \epsilon^*[(r/r^*)^{-12} - 2(r/r^*)^{-6}], \qquad (2.2)$$

where r^* and ϵ^* are the radius and well depth of the

[4] M. H. Rice, R. G. McQueen, and J. M. Walsh, *Solid State Physics*, edited by F. Seitz and D. Turnbull (Academic Press Inc., New York, 1958), Vol. 6.

[5] J. Dapoigny, J. Kieffer, and B. Vodar, J. Phys. radium 8, 733 (1955).

[6] L. E. Lennard-Jones and A. F. Devonshire, Proc. Roy. Soc. (London) A163, 53 (1937).

[7] See, for example, R. Cournat and K. O. Friedrichs, *Supersonic Flow and Shock Waves* (Interscience Publishers, Inc., New York, 1948). p. 121 ff.

[8] F. Din, *Thermodynamic Functions of Gases* (Butterworths Scientific Publications Ltd., London, 1956), Vol. 2, p. 181.

potential, and $u(r)$ is the potential at the separation r. The isotherms are shown in Figs. 1(a) and 1(b). In order to obtain a convenient scale, the values of E'/RT and $PV/RT - 1$ for the regular (face-centered cubic) lattice configuration have been subtracted off. For this form of the pair potential, these are given by[9]

$$E'/RT = 6[1.0110(r/r^*)^{-12} - 2.4090(r/r^*)^{-6}]$$
$$PV/RT - 1 = 24[1.0110(r/r^*)^{-12} - 1.2045(r/r^*)^{-6}]. \quad (2.3)$$

The calculation of points on the Hugoniot curve from these results was done by interpolation in temperature at constant volume and vice versa. In the constant-volume method, the Hugoniot function, the left-hand side of Eq. (2.1a), was calculated for each reduced temperature at the given volume. Three-point interpolation was then used to find the temperature at which Eq. (2.1a) was satisfied, and the remaining equation-of-state quantities were also obtained by interpolation.

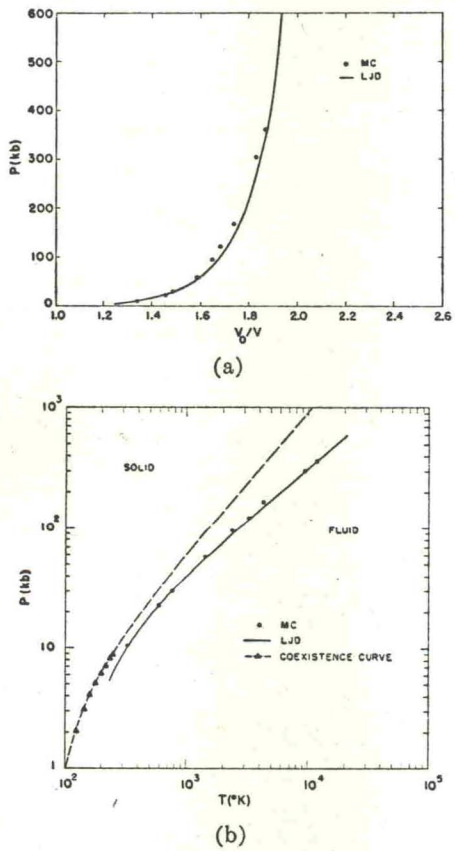

FIG. 2. Shock Hugoniots for liquid argon calculated with Monte Carlo (MC) and LJD equations of state using the same pair potential [Eqs. (2.2) and (2.4)]. The pressure colume plane is shown in (a), and the pressure-temperature plane in (b). Also shown in (b) are some experimental points on the fluid-solid coexistence curve and its extrapolation by means of the empirical Simon relation.

[9] J. E. Jones and A. E. Ingham, Proc. Roy. Soc. (London) **A107**, 636 (1925).

TABLE I. Shock Hugoniots calculated from the Monte Carlo equation-of-state [with Lennard-Jones potential, Eq. (2.4)].

$P(kb)$	V/V_0	T(°K)
362	0.535	11 900
305	0.547	9 360
168	0.572	4 330
123	0.595	3 120
96	0.606	2 390
59	0.631	1 401
30	0.673	760
23	0.687	569

Interpolation in volume at constant temperature was complicated by the shape of the isotherms. The probable first-order phase transition, discussed in reference 3 for the isotherm with $kT/\epsilon^* = 2.74$, appears to be present on the higher isotherms also. Because of the small number of points on these isotherms, the dashed curves shown in Figs. 1(a) and 1(b) were sketched in, using only a discontinuity in slope to represent the probable transition. A Hugoniot point on each isotherm was then obtained by interpolation at constant temperature. (On the lowest isotherm, the Monte Carlo points were used directly with three-point interpolation.) As a check on these methods, a Hugoniot point was calculated by the first method from the LJD isotherms of Fig. 1 and found to be in good agreement with an explicit calculation.

In order to transform from reduced thermodynamic variables to real ones, a set of pair potential parameters close to those obtained from second-virial coefficient data were used[10]:

$$\epsilon^*/k = 119.3\ °\text{K}, \qquad r^* = 3.833\ \text{A}, \quad (2.4)$$

where k is Boltzmann's constant.

The resulting Hugoniot curve is given in Table I and in Figs. 2(a) and 2(b). Also shown in Fig. 2(b) is the extrapolation of the experimental solid-liquid coexistence curve by means of the empirical Simon relation.[11] From this graph it appears that the Hugoniot lies entirely in the fluid region. To shed further light on this point, the loci of Hugoniot points were added to Figs. 1(a) and 1(b). Although the position of the probable transition is poorly

[10] E. Whalley and W. G. Schneider, J. Chem. Phys. **23**, 1644 (1955).

[11] D. W. Robinson, Proc. Roy. Soc. (London) **A225**, 393 (1954).

determined by the Monte Carlo results, it appears that the lower portion of the Hugoniot curve may lie in the solid region. As pointed out in reference 3, the apparent coexistence point on the lowest-temperature Monte Carlo isotherm is at a lower pressure than that predicted by the extrapolation of the experimental results. Thus the coexistence curve predicted by the Monte Carlo results probably lies somewhat to the right of the dashed curve of Fig. 2(b) and intersects the lower portion of the Hugoniot curve.

TABLE II. Shock Hugoniots calculated with the LJD equation of state.

	Lennard-Jones potential [Eq. (2.4)]		Exp-six potential [Eq. (3.1)]		Exp-six potential [Eq. (3.2)]	
$P(kb)$	V/V_0	T(°K)	V/V_0	T(°K)	V/V_0	T(°K)
600	0.5137	21 230	0.4698	20 900	0.4121	22 863
500	0.5205	17 210	0.4791	16 920	0.4228	18 420
400	0.5292	13 310	0.4907	13 053	0.4359	14 195
300	0.5409	9 555	0.5062	9 335	0.4528	10 177
250	0.5487	7 743	0.5164	7 547	0.4638	8 244
200	0.5587	5 988	0.5292	5 819	0.4775	6 370
150	0.5722	4 306	0.5464	4 167	0.4957	4 570
100	0.5927	2 720	0.5720	2 616	0.5228	2 872
75	0.6083	1 976	0.5912	1 893	0.5430	2 077
50	0.6322	1 280	0.6199	1 221	0.5732	1 334
25	0.6778	652.5	0.6730	620.2	0.6291	668.6
20	0.6938	538.7	0.6911	512.6	0.6482	548.9
15	0.7151	430.0	0.7150	410.3	0.6734	435.4
10	0.7462	327.0	0.7494	314.2	0.7096	328.8
5	0.8003	229.4	0.8082	223.8	0.7716	229.4

The same set of isotherms and the shock Hugoniot were also calculated from the LJD cell theory.[6] These calculations were done on the IBM 704. The Hugoniot curve was obtained by the iterative solution of Eq. (2.1), with the equation-of-state points calculated as needed. The results are given in Table II and are compared with the Monte Carlo results in Figs. 1 and 2.

Although the isotherms do not agree too well, particularly on the fluid side of the phase transition (which is of course not predicted by the cell theory), the two Hugoniot curves are quite close. Of course the isotherms shown give only the difference between the E or PV and the contributions of the regular lattice configuration, which is the same in both calculations. Examination of the results, shows, however, that the lattice values are less than half of the total above about 50 kb on the Hugoniot, so that the fact that the lattice contributions are the same cannot alone account for the agreement. It appears that the agreement is due mainly to the cancellation of the differences in PV and E when they are subtracted in the Hugoniot equation, plus

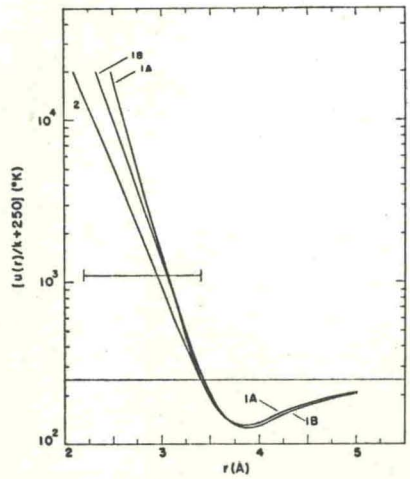

FIG. 3. Intermolecular potentials used in the calculations. (1A) Lennard-Jones 6–12, constants from second virial coefficient data [Eq. (2.4)] $\epsilon^*/k = 119.3$ °K. $r^* = 3.833$. (1B) Exp-six, constants from second virial coefficient and crystal data [Eq. (3.1)] $\alpha = 14$, $\epsilon^*/k = 123.2$ °K, $r^* = 3.866$ A. 2. Exp-six, constants from molecular scattering data for 2.2 A $< r <$ 3.4 A [Eq. (3.2)] $\alpha = 12$, $\epsilon^*/k = 116$, $r^* = 3.87$A. The range of distances covered by the scattering data is indicated by the vertical bars. To the right of the minimum, the attractive portion, not shown, lies between curves 1A and 1B.

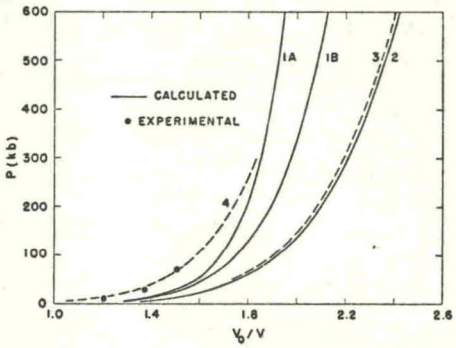

FIG. 4. Shock Hugoniots for liquid argon calculated with different pair potentials: Curves 1A, 1B, and 2 correspond to the potentials of Fig. 3. Curves 3 and 4 illustrate the effect of varying the potential parameters: 3. $\alpha = 12$, $\epsilon^*/k = 123.2$, $r^* = 3.866$. 4. $\alpha = 14$, $\epsilon^*/k = 123.2$, $r^* = 4.18$ A. Curve 4 also illustrates the change in r^* required to reproduce the available experimental data.

the fact that a part of the Hugoniot curve corresponds to a region in which the LJD and Monte Carlo isotherms are crossing.

3. EFFECT OF THE PAIR POTENTIAL

In addition to the Lennard-Jones form of the pair potential used above, the exp-six form has also been fit to second virial coefficient and crystal data, with the result[12]

$$u(r) = \frac{\epsilon^*}{1 - 6/\alpha}\left[\frac{6}{\alpha}e^{\alpha(1-r/r^*)} - \left(\frac{r}{r^*}\right)^{-6}\right] \qquad (3.1a)$$

[12] E. W. Mason and W. E. Rice, J. Chem. Phys. 22, 843 (1954).

$\alpha = 14, \epsilon^*/k = 123.2\ °\text{K}, r^* = 3.866\ \text{A}.$ (3.1b)

The repulsive portions of these two potentials (Lennard-Jones and exp-six) differ somewhat, but are both much "harder" than the molecular scattering results of Mason and Amdur,[2] who have found that the exp-six form with

$\alpha = 12, \quad \epsilon^*/k = 116\ °\text{K}, \quad r^* = 3.87\ \text{A},$ (3.2)

reproduces the molecular scattering data quite well and has an attractive portion quite close to that of Eq. (3.1). This potential is undoubtedly the most nearly correct one for the present calculations, in which the repulsive portion dominates.

Therefore, we have used the LJD equation of state to calculate the shock Hugoniot of liquid argon using this potential as well as those determined from second virial coefficient data, Eqs. (3.1) and (2.2), (2.4). These pair potentials are shown in Fig. 3, and the corresponding shock Hugoniots are given in Table II and Fig. 4.

In order to illustrate the effects of changing the adjustable parameters in the potential function, the dashed curves of Fig. 4 were calculated. The effect of changing α only, in Eq. (3.1a) can be seen by comparing curves 1B and 3; of changing ϵ^* only, by comparing 2 and 3; and of changing r^* only, by comparing 1B and 4. Curve 4 is also used for another purpose below.

In all of the calculated Hugoniots except that shown in Fig. 2, only a single shell of neighbors was included in the calculation of the cell partition function. In calculating the lattice energy, all shells of neighbors were included for the Lennard-Jones potential, but for the exp-six potential only one shell was included in the repulsive term. This was done partly for simplicity, since for an exponential repulsion the ratio of the entire lattice energy to the single-shell energy is a fairly strongly increasing function of density. Also, it seems likely that the inclusion of all shells in the calculation of the repulsive energy would probably give too large a result at high densities, since the exponential term remains relatively large at intermediate distances.*

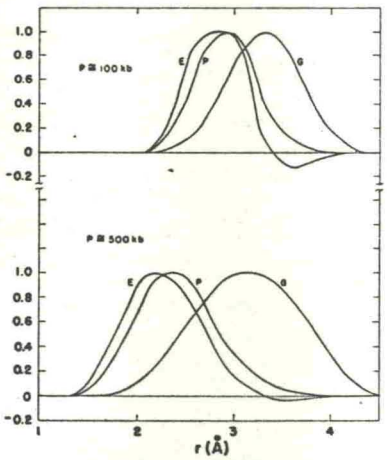

FIG. 5. Normalized weighting functions and integrands for the LJD cell integrals transformed to the form of integrals over the intermolecular separation r. Upper curves: for $P \cong$ 100kb on the shock Hugoniot 2 of Fig. 4; lower curves: for $P \cong$ 500kb on the same shock Hugoniot. Here G is the weighting function, P is the integrand for $(PV/RT - 1)$ and E is the integrand for E'/RT.

4. DISCUSSION

In order to show the relative importance of different intermolecular distances in these calculations, we have obtained in the appendix a weighting function which gives the relative weight with which each intermolecular distance occurs in the cell integrals of the LJD equation of state. This weighting function is given in Eq. (A12), and can be regarded as a pseudo radial distribution function in the sense that it gives the LJD equation of state when it is used in place of the radial distribution function $g(r)$ in the general statistical mechanical expressions for pressure and excess internal energy

$$\frac{E'}{RT} = \frac{2\pi N}{VkT}\int_0^\infty u(r)g(r)r^2\,dr \qquad (4.1)$$

$$\frac{PV}{RT} - 1 = -\frac{2\pi N}{VkT}\frac{1}{3}\int_0^\infty \frac{du(r)}{dr}\,g(r)r^3\,dr.$$

The weighting function consists of the sum of a continuous function and a Dirac delta-function. The continuous portion of the normalized weighting function and the corresponding integrands of Eqs. (4.1) are plotted in Fig. 5 for values of T and V corresponding to pressures of about 100 and 500 kb on curve 2 of Fig. 4. The delta-function (not shown) lies at the maximum of the weighting function, and has the opposite sign and an area equal to half that under the weighting function curve. As expected, the repulsive portion of the potential is the determining factor, and the range of distances of greatest importance coincides roughly with the range of the molecular scattering results shown in Fig. 3.

The available experimental measurements of the shock Hugoniot[5] consist of x-ray densitometry measurements of the density behind the shock wave.

* In order to obtain some idea of the effect of omitting the second and third shells of neighbors in calculating the cell integrals, the Hugoniot curve of Fig. 2 was also calculated in this way. The resulting curve was displaced slightly to the right—by about 0.01 in V_0/V.

The effect of omitting the additional shells of neighbors in calculating the lattice contribution for the repulsive term of the exp-six potential is somewhat smaller than this.

and extend to about 70 kb. They are compared with the calculated curves in Fig. 4. In order to see what changes in the potential would have to be made to give a calculated curve through these points, we took as a starting point the second-virial-coefficient exp-six potential, Eq. (3.1). An increase of r^* to 4.18 A at constant α and ϵ^*/k was required to match the experimental data; these values gave curve 4 of Fig. 3. An increase of ϵ^*/k to 240 °K at constant α and r^* gave a calculated curve which would be nearly indistinguishable from curve 4 if plotted in Fig. 3. It seems unlikely that the assumption of additivity of pair forces could fail so badly at these low pressures as to require such a major adjustment of the pair potential in order to match the experimental data. For this reason, and because data at higher pressures would be of considerable interest, similar experiments carried to higher pressures would be desirable.

ACKNOWLEDGMENT

This work was performed under the auspices of the United States Atomic Energy Commission.

APPENDIX

In working with an equation of state based on a pair potential $u(r)$, it is desirable to have the energy expressed in the form

$$E = \int_0^\infty u(r)h(r)\,dr, \tag{A1}$$

so that the function $h(r)$ gives immediately the relative importance of different intermolecular distances.

The cell integrals of the LJD equation of state can be transformed into this form. The expressions for internal energy and pressure can be written (for nearest-neighbor interactions)

$$PV - RT = -N[\tfrac{1}{6}Ztf'(t) - g(\tfrac{1}{3}t\omega_t)/g(1)] \tag{A2a}$$

$$E' = N[\tfrac{1}{2}Zf(t) = g(\omega)/g(1)], \tag{A2b}$$

where Z is the coordination number, $t = a/r^*$ with a the nearest-neighbor distance, the prime denotes differentiation, and the subscript t denotes partial differentiation with respect to t. The pair potential has been written with a reduced argument: $f(r/r^*) = u(r)$. The cell potential ω is defined by

$$\omega(x, t) = \frac{Z}{2x}\int_{1-x}^{1+x} x'[f(tx') - f(t)]\,dx', \tag{A3}$$

and the g function by the cell integral

$$g(z) = 2\int_0^b [z]x^2 e^{-\omega(x,t)/kT}\,dx, \tag{A4}$$

where b is the cell radius in units of a.

By defining $\varphi(x, t) = \exp[-\omega(x, t)/kT]$, and making use of Eq. (A3), the cell integral for the energy becomes

$$g(\omega) = Z\int_0^b dx\int_{1-x}^{1+x} dx' x\varphi(x, t)x'[f(tx') - f(t)]. \tag{A5}$$

Reversal of the order of integration gives

$$g(\omega) = Z\int_{1-b}^{1+b} dx'\int_{|1-x'|}^{b} dx\, x'[f(tx') - f(t)]x\varphi(x, t), \tag{A6}$$

or

$$g(\omega) = Z\left\{\int_{1-b}^{1+b} f(tx')G(x', t)\,dx' - f(t)\int_{1-b}^{1+b} G(x', t)\,dx'\right\}, \tag{A7}$$

where

$$G(x', t) = x'\int_{|1-x'|}^{b} x\varphi(x, t)\,dx. \tag{A8}$$

It is easy to show that

$$\int_{1-b}^{1+b} G(x', t)\,dx' = g(1), \tag{A9}$$

and we thus obtain from Eq. (A2b)

$$E' = NZ\left[-\frac{f(t)}{2} + \int_{1-b}^{1+b} f(tx')\frac{G(x', t)}{g(1)}\,dx'\right]. \tag{A10}$$

The corresponding expression for the pressure is obtained in similar fashion,

$$PV - RT = -NZ\left[\tfrac{1}{6}tf'(t) - \int_{1-b}^{1+b}\tfrac{1}{3}tx'f'(tx')\frac{G(x', t)}{g(1)}\,dx'\right]. \tag{A11}$$

It is convenient to express the desired weighting function in a form analogous to the radial distribution function:

$$h(r) = \frac{Z}{2\pi\sqrt{2}x'^2}\left[\frac{G(x', t)}{g(1)} - \tfrac{1}{2}\,\delta(x' - 1)\right]; \qquad x' = r/a \tag{A12}$$

with $G(x', t) = 0$ for $x' < 1 - b$ and $x' > 1 + b$, and δ the Dirac δ-function. If $h(r)$ is used instead of $g(r)$ in the usual statistical mechanical expressions for the energy and pressure, Eqs. (4.1), the results are just the LJD expressions for pressure and energy, Eqs. (A2).